CLASSIFICATION OF 3D URBAN SCENES
A Voxel based Approach

Ahmad Kamal Aijazi[1,2], Paul Checchin[1,2] and Laurent Trassoudaine[1,2]

[1] *Clermont Université, Université Blaise Pascal, Institut Pascal, BP 10448, F-63000 Clermont-Ferrand, France*

[2] *CNRS, UMR 6602, Institut Pascal, F-63171 Aubiere, France*

Keywords: 3D point cloud segmentation, Hybrid data, Super-Voxels, Urban scene classification.

Abstract: In this paper we present a method to classify urban scenes based on a super-voxel segmentation of sparse 3D data. The 3D point cloud is first segmented into voxels, which are then joined together by using a link-chain method rather than the usual region growing algorithm to create objects. These objects are then classified using geometrical models and local descriptors. In order to evaluate our results a new metric is presented, which combines both segmentation and classification results simultaneously. The effects of voxel size and incorporation of RGB color and intensity on the classification results are also discussed.

1 INTRODUCTION

The automatic segmentation and classification of 3D urban data have gained widespread interest and importance in the scientific community due to the increasing demand of urban landscape analysis and cartography for different popular applications, coupled with the advances in 3D data acquisition technology. The automatic extraction (or partially supervised) of important urban scene structures such as roads, vegetation, lamp posts, and buildings from 3D data has been found to be an attractive approach to urban scene analysis because it can tremendously reduce the resources required in analyzing the data for subsequent use in 3D city modeling and other algorithms.

A common way to quickly collect 3D data of urban environments is by using an airborne LiDAR (Sithole and Vosselman, 2004), (Verma et al., 2006), where the LiDAR scanner is mounted in the bottom of an aircraft. Although this method generates a 3D scan in a very short time period, there are a number of limitations in 3D urban data collected from this method such as a limited viewing angle.

These limitations are overcome by using a mobile terrestrial or ground based LiDAR system in which unlike the airborne LiDAR system, the 3D data obtained is dense and the point of view of the images is closer to the urban landscapes. However this offers both advantages and disadvantages when processing the data. The disadvantages include the demand for more processing power required to handle the increased volume of 3D data. On the other hand, the advantage is the availability of a more detailed sampling of the object's lateral views, which provides a more comprehensive model of the urban structures including building facades, lamp posts, etc.

Our work revolves around the segmentation and then classification of ground based 3D data of urban scenes. The aim is to provide an effective preprocessing step for different subsequent algorithms or as an add-on boost for more specific classification algorithms.

2 RELATED WORK

In order to fully exploit 3D point clouds, effective segmentation has proved to be a necessary and critical pre-processing step in a number of autonomous perception tasks.

Earlier works including (Anguelov et al., 2005), (Lim and Suter, 2007) and (Munoz et al., 2009) used small sets of specialized features, such as local point density or height from the ground, to discriminate only few object categories in outdoor scenes, or to separate foreground from background. Lately, segmentation has been commonly formulated as graph clustering. Instances of such approaches are Graph-Cuts including Normalized-Cuts and Min-Cuts.

(Golovinskiy and Funkhouser, 2009) extended Graph-Cuts segmentation to 3D point clouds by us-

Aijazi A., Checchin P. and Trassoudaine L. (2012).
CLASSIFICATION OF 3D URBAN SCENES - A Voxel based Approach.
In *Proceedings of the 1st International Conference on Pattern Recognition Applications and Methods*, pages 61-70
DOI: 10.5220/0003733100610070

ing k-Nearest Neighbors (k-NN) to build a 3D graph. In this work edge weights based on exponential decay in length were used. But the limitation of this method is that it requires prior knowledge of the location of the objects to be segmented.

Another segmentation algorithm for natural images, recently introduced by Felzenszwalb and Huttenlocher (FH) (Felzenszwalb and Huttenlocher, 2004), has gained popularity for several robotic applications due to its efficiency. (Zhu et al., 2010) presented a method in which a 3D graph is built with k-NN while assuming the ground to be flat for removal during pre-processing. 3D partitioning is then obtained with the FH algorithm. We have used the same assumption.

(Triebel et al., 2010) modified the FH algorithm for range images to propose an unsupervised probabilistic segmentation technique. In this approach, the 3D data is first over-segmented during pre-processing. (Schoenberg et al., 2010) have applied the FH algorithm to colored 3D data obtained from a co-registered camera laser pair. The edge weights are computed as a weighted combination of Euclidean distances, pixel intensity differences and angles between surface normals estimated at each 3D point. The FH algorithm is then run on the image graph to provide the final 3D partitioning. The evaluation of the algorithm is done on road segments only.

(Strom et al., 2010) proposed a similar approach but modified the FH algorithm to incorporate angle differences between surface normals in addition to the differences in color values. Segmentation evaluation was done visually without ground truth data. Our approach differs from the above mentioned methods as, instead of using the properties of each point for segmentation resulting in over segmentation, we have grouped the 3D points based on Euclidian distance into voxels and then assigned normalized properties to these voxels transforming them into super-voxels. This not only prevents over segmentation but in fact reduces the data set by many folds thus reducing post-processing time.

A spanning tree approach to the segmentation of 3D point clouds was proposed in (Pauling et al., 2009). Graph nodes represent Gaussian ellipsoids as geometric primitives.

These ellipsoids are then merged using a tree growing algorithm. The resulting segmentation is similar to a super-voxel type of partitioning with voxels of ellipsoidal shapes and various sizes. Unlike this method, our approach uses cuboids of different shapes and sizes as geometric primitives and a link-chain method to group them together. In the literature survey we also find some segmentation methods based on surface discontinuities such as (Moosmann et al., 2009) who used surface convexity in a terrain mesh as a separator between objects.

In the past, research related to 3D urban scene classification and analysis had been mostly performed using either 3D data collected by airborne LiDAR for extracting bare-earth and building structures (Lu et al., 2009) (Vosselman et al., 2005) or 3D data collected from static terrestrial laser scanners for extraction of building features such as walls and windows (Pu and Vosselman, 2009). In (Lam et al., 2010) the authors extracted roads and objects just around the roads like road signs. They used a least square fit plane and RANSAC method to first extract a plane from the points followed by a Kalman filter to extract roads in an urban environment. A method of classification based on global features is presented in (Halma et al., 2010) in which a single global spin image for every object is used to detect cars in the scene while in (Rusu et al., 2010) a Fast Point Feature Histogram (FPFH) local feature is modified into global feature for simultaneous object identification and view-point detection. Classification using local features and descriptors such as Spin Image (Johnson, 1997), Spherical Harmonic Descriptors (Kazhdan et al., 2003), Heat Kernel Signatures (Sun et al., 2009), Shape Distributions (Osada et al., 2002), 3D SURF feature (Knopp et al., 2010) is also found in the literature survey. There is also a third type of Classification based on Bag Of Features (BOF) as discussed in (Liu et al., 2006). In (Lim and Suter, 2008) a method of multi-scale Conditional Random Fields is proposed to classify 3D outdoor terrestrial laser scanned data by introducing regional edge potentials in addition to the local edge and node potentials in the multi-scale Conditional Random Fields. This is followed by fitting plane patches onto the labeled objects such as building terrain and floor data using the RANSAC algorithm as a post-processing step to geometrically model the scene. (Douillard et al., 2009) presented a method in which 3D points are projected on to the image to find regions of interest for classification.

In our work we use geometrical models based on local features and descriptors to successfully classify different segmented objects represented by groups of voxels in the urban scene. Ground is assumed to be flat and is used as an object separator. Our segmentation technique is discussed in Section 3. Section 4 deals with the classification of these segmented objects. In Section 5 a new evaluation metric is introduced to evaluate both segmentation and classification together while in Section 6 we present the results of our work. Finally, we conclude in Section 7.

3 VOXEL SEGMENTATION

3.1 Voxelisation of Data

When dealing with large 3D data sets, the computational cost of processing all the individual points is very high, making it unpractical for real time applications. It is therefore sought to reduce these points by grouping or removing redundant or un-useful points together. Similarly, in our work the individual 3D points are clustered together to form a higher level representation or voxel as shown in Figure 1.

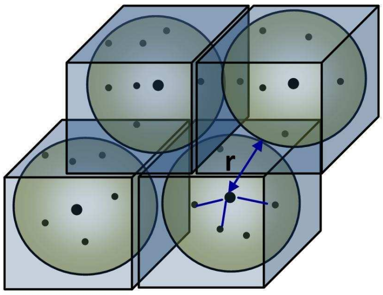

Figure 1: A number of points is grouped together to form cubical voxels of maximum size $2r$. The actual voxel sizes vary according to the maximum and minimum values of the neighboring points found along each axis to ensure the profile of the structure.

For p data points, a number of s voxels, where $s << p$, are computed based on k-NN with $w = 1/d$ given as the weight to each neighbor (where d is the distance to the neighbor). Let P and Q be two points in the X, Y and Z coordinate system then d is given as:

$$d = \sqrt{(P_X - Q_X)^2 + (P_Y - Q_Y)^2 + (P_Z - Q_Z)^2} \quad (1)$$

The maximum size of the voxel $2r$, where r is radius of ellipsoid, depends upon the density of the 3D point cloud. In (Lim and Suter, 2008) color values are also added in this step but it is observed that for relatively smaller voxel sizes, the variation in properties such as color is not much and just increases computational cost. For these reasons we have only used distance as a parameter in this step and the other properties in the next step of clustering the voxels to form objects. Also we have ensured that each 3D point which belongs to a voxel is not considered for further voxelisation. This not only prevents over segmentation but also reduces processing time.

For the voxels we use a cuboid because of its symmetry which avoids fitting problems while grouping and also minimizes the effect of voxel shape during feature extraction.

Although the maximum voxel size is predefined, the actual voxel sizes vary according to the maximum and minimum values of the neighboring points found along each axis to ensure the profile of the structure.

Once these voxels are created we find the properties of each voxel. These properties include surface normals, RGB-color, intensity, geometric primitives such as barycenter, geometrical center, maximum and minimum values along each axis, etc. Where some of these properties are averaged and normalized values of the constituting points, the surface normals are calculated using PCA (Principal Component Analysis). The PCA method has been proved to perform better than the area averaging method (Klasing et al., 2009) to estimate the surface normal.

Given a point cloud data set $\mathcal{D} = \{x_i\}_{i=1}^{n}$, the PCA surface normal approximation for a given data point $p \in \mathcal{D}$ is typically computed by first determining the k-Nearest Neighbors, $x_k \in \mathcal{D}$, of p. Given the K neighbors, the approximate surface normal is then the eigenvector associated with the smallest eigenvalue of the symmetric positive semi-definite matrix

$$\mathbf{P} = \sum_{k=1}^{K} (x_k - \overline{p})^T (x_k - \overline{p}) \quad (2)$$

where $\overline{p}$ is the local data centroid: $\overline{p} = \frac{1}{K}\sum_{j=1}^{K} x_j$.

The estimated surface normal is ambiguous in terms of sign; to account for this ambiguity the dot product between estimated surface normals is repeated using the negative estimated surface normal of one of the vectors and the minimum result of the term is selected. Yet for us the sign of the normal vector is not important as we are more interested in the orientation. Using this method, a single surface normal is estimated for all the points belonging to a voxel and is then associated with that particular voxel along with the other properties, transforming it into a super-voxel.

All these properties would then be used in grouping these super-voxels into objects and then during the classification of these objects. Instead of using thousands of points in the data set, the advantage of this approach is that we can now use the reduced number of super-voxels to obtain similar results for classification and other algorithms. In our case, the data sets of $110,392$, $53,676$ and $27,396$ points were reduced to $18,541$, $6,928$ and $7,924$ super-voxels respectively which were then used for subsequent processing.

3.2 Clustering by Link-chain Method

When the 3D data is converted into super-voxels, the next step is to group these super-voxels to segment into distinct objects.

Usually for such tasks a region growing algorithm (Vieira and Shimada, 2005) is used in which the properties of the whole growing region may influence the boundary or edge conditions. This may sometimes lead to erroneous segmentation. Also common in such type of methods is a node based approach (Moosmann et al., 2009) in which at every node, boundary conditions have to be checked in all 5 different possible directions. In our work we have proposed a link-chain method instead to group these super-voxels together into segmented objects.

In this method each super-voxel is considered as a link of a chain. All secondary links attached to each of these principal links are found. In the final step all the principal links are linked together to form a continuous chain removing redundant secondary links in the process as shown in Figure 2.

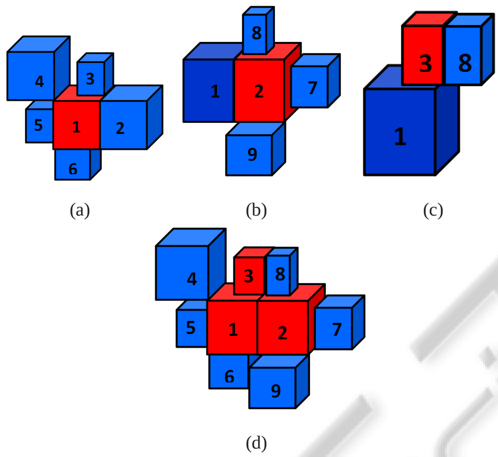

Figure 2: Clustering of super-voxels using a link-chain method is demonstrated. (a) shows super-voxel 1 taken as principal link in red and all secondary links attached to it in blue. (b) and (c) shows the same for super-voxel 2 and 3 taken as principal links. (d) shows the linking of principal links (super-voxels 1, 2 & 3) to form a chain removing redundant secondary links.

Let $\mathbf{V}_P$ be a principal link and $\mathbf{V}_n$ be the n number of secondary links then each of the $\mathbf{V}_n$ is linked to $\mathbf{V}_P$ if and only if the following three conditions are fulfilled:

$$\left|\mathbf{V}_{P_{X,Y,Z}} - \mathbf{V}_{n_{X,Y,Z}}\right| \leq (w_D + c_D) \tag{3}$$

$$\left|\mathbf{V}_{P_{R,G,B}} - \mathbf{V}_{n_{R,G,B}}\right| \leq 3\sqrt{w_C} \tag{4}$$

$$\left|\mathbf{V}_{P_I} - \mathbf{V}_{n_I}\right| \leq 3\sqrt{w_I} \tag{5}$$

where, for the principal and secondary link super-voxels respectively:

- $\mathbf{V}_{P_{X,Y,Z}}$, $\mathbf{V}_{n_{X,Y,Z}}$ are the geometrical centers;
- $\mathbf{V}_{P_{R,G,B}}$, $\mathbf{V}_{n_{R,G,B}}$ are the mean RGB values;
- $\mathbf{V}_{P_I}$, $\mathbf{V}_{n_I}$ are the mean intensity values;
- w_C is the color weight equal to the maximum value of the variances $Var(R,G,B)$;
- w_I is the intensity weight equal to the maximum value of the variances $Var(I)$.

w_D is the distance weight given as $\frac{\left(\mathbf{V}_{P_{s_{X,Y,Z}}} + \mathbf{V}_{n_{s_{X,Y,Z}}}\right)}{2}$. Here $s_{X,Y,Z}$ is the voxel size along X, Y & Z axis respectively.

c_D is the inter-distance constant (along the three dimensions) added depending upon the density of points and also to overcome measurement errors, holes and occlusions, etc. The value of c_D needs to be carefully selected depending upon the data.

The orientation of normals is not considered in this stage to allow the segmentation of complete objects as one entity instead of just planar faces.

This segmentation method ensures that only the adjacent boundary conditions are considered for segmentation with no influence of a distant neighbor's properties. This may prove to be more adapted to sharp structural changes in the urban environment. The segmentation algorithm is summarized in Algorithm 1.

Algorithm 1: Segmentation.

repeat
  Select a 3D point for voxelisation
  Find all neighboring points to be included in the voxel using k-NN within the maximum voxel length specified
  Find all properties of the super-voxel including surface normal found by using PCA
until all 3D points are used in a voxel
repeat
  Specify a super-voxel as a principal link
  Find all secondary links attached to the principal link
until all super-voxels are used
Link all principal links to form a chain removing redundant links in the process

With this method 18,541, 6,928 and 7,924 super-voxels obtained from processing 3 different data sets were successfully segmented into 237, 75 and 41 distinct objects respectively.

4 CLASSIFICATION OF OBJECTS

In order to classify these objects, we assume the ground to be flat and use it as separator between objects. For this purpose we first classify and segment out the ground from the scene and then the rest of the objects. This step leaves the remaining objects as if suspended in space, i.e distinct and well separated, making them easier to be classified as shown in Figure 3.

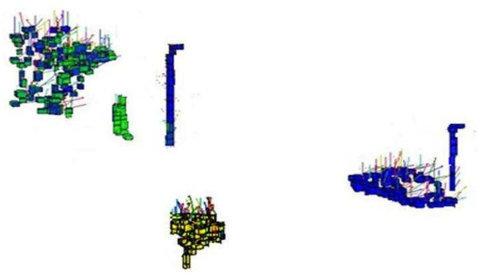

Figure 3: Segmented objects in a scene with prior ground removal.

The ground or roads followed by these objects are then classified using geometrical and local descriptors. These mainly include:

a. Surface Normals. The orientation of the surface normals is essential for classification of ground and building faces. For ground object the surface normals are along Z-axis (height axis) whereas for building faces the surface normals are parallel to the X-Y axis (ground plane), see Figure 4.

b. Geometrical Center and Barycenter. The height difference between the geometrical center and the barycenter along with other properties is very useful in distinguishing objects like trees and vegetation, etc., where:

$$h(\text{barycenter} - \text{geometrical center}) > 0$$

with h being the height function.

c. Color and Intensity. Intensity and color are also an important discriminating factor for several objects.

d. Geometrical Shape. Along with the above mentioned descriptors, geometrical shape plays an important role in classifying objects. In 3D space, where pedestrians and pole are represented as long and thin with poles being longer, cars and vegetation are broad and short. Similarly, as roads represent a low flat plane, the buildings are represented as large (both in width and height) vertical blocks.

Using these descriptors we successfully classify urban scenes into 5 different classes (mostly present in our scenes) i.e. buildings, roads, cars, poles and trees. The classification results and a new evaluation metric are discussed in the following sections.

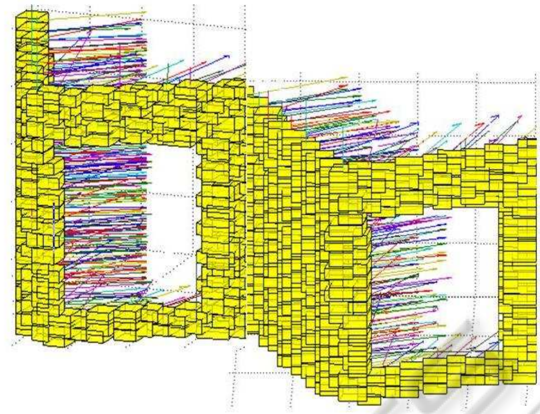

(a) Normals of building.

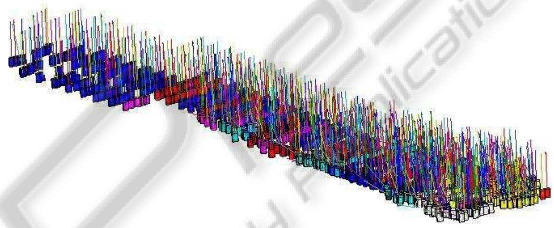

(b) Normals of road.

Figure 4: (a) shows surface normals of building super-voxels are parallel to the ground plane. In (b) it can be clearly seen that the surface normals of road surface super-voxels are perpendicular to the ground plane.

5 EVALUATION METRICS

In previous works, different evaluation metrics are introduced for both segmentation results and classifiers independently. Thus in our work we present a new evaluation metric which incorporates both segmentation and classification together.

The evaluation method is based on comparing the total percentage of super-voxels successfully classified as a particular object. Let T_i, $i \in \{1, \cdots, N\}$, be the total number of super-voxels distributed into objects belonging to N number of different classes, i.e this serves as the ground truth, and let t_{j_i}, $i \in \{1, \cdots, N\}$, be the total number of super-voxels classified as a particular class of type-j and distributed into objects belonging to N different classes (for example a super-voxel classified as part of the building class may actually belong to a tree) then the ratio S_{jk} (j is the class type as well as the row number of the matrix and $k \in \{1, \cdots, N\}$) is given as:

$$S_{jk} = \frac{t_{j_k}}{T_k}$$

These values of S_{jk} are calculated for each type of class and are used to fill up each element of the confusion matrix, row by row (refer to Table 1 for instance). Each row of the matrix represents a particular class.

Thus, for a class of type-1 (i.e. first row of the matrix) the values of:

True Positive rate, $\mathbf{TP} = S_{11}$ (i.e the diagonal of the matrix represents the **TP**s)

False Positive rate, $\mathbf{FP} = \sum_{m=2}^{N} S_{1m}$

True Negative rate, $\mathbf{TN} = (1 - \mathbf{FP})$

False Negative rate, $\mathbf{FN} = (1 - \mathbf{TP})$

The diagonal of this matrix or **TP**s gives the Segmentation ACCuracy **SACC**, similar to the voxel scores recently introduced by (Douillard et al., 2011). The effects of unclassified super-voxels are automatically incorporated in the segmentation accuracy. Using the above values the Classification ACCuracy **CACC** is given as:

$$\mathbf{CACC} = \frac{\mathbf{TP} + \mathbf{TN}}{\mathbf{TP} + \mathbf{TN} + \mathbf{FP} + \mathbf{FN}} \tag{6}$$

This value of **CACC** is calculated for all N types of classes of objects present in the scene. Overall Classification ACCuracy **OCACC** can then be calculated as

$$\mathbf{OCACC} = \frac{1}{N} \sum_{i=1}^{N} \mathbf{CACC}_i \tag{7}$$

where N is the total number of object classes present in the scene. Similarly, the Overall Segmentation ACCuracy **OSACC** can also be calculated.

The values of T_i and t_{j_i} used above are laboriously calculated by hand matching the voxelised data output and the final classified super-voxels and points.

6 RESULTS

Our algorithm was validated on 3D data acquired from different urban scenes on the Campus of University Blaise Pascal in Clermont-Ferrand, France. The results of three such data sets are discussed here. The data sets consisted of $27,396$, $53,676$ and $110,392$ 3D points respectively. These 3D points were coupled with corresponding RGB and intensity values. The results are now summarized.

6.1 Data Set 1

The data set consisting of $27,396$ data points was reduced to $7,924$ super-voxels keeping maximum voxel size 0.3 m and $c_D = 0.25$ m. These super-voxels are then segmented into 41 distinct objects. The classification result of these objects is shown in Figure 5 and in Table 1.

Table 1: Classification results of data set 1 in the new evaluation metrics.

	Building	Road	Tree	Pole	Car	**CACC**
Building	0.943	0.073	0	0	0	0.935
Road	0.007	0.858	0.015	0.008	0	0.914
Tree	0	0.025	0.984	0	0	0.979
Pole	0	0.049	0	0.937	0	0.944
Car	–	–	–	–	–	–
Overall segmentation accuracy: **OSACC**					0.930	
Overall classification accuracy: **OCACC**						0.943

6.2 Data Set 2

The data set consisting of $53,676$ data points was reduced to $6,928$ super-voxels keeping maximum voxel size 0.3 m and $c_D = 0.25$ m. These super-voxels are then segmented into 75 distinct objects. The classification result of these objects is shown in Figure 6 and in Table 2.

Table 2: Classification results of data set 2 in the new evaluation metrics.

	Building	Road	Tree	Pole	Car	**CACC**
Building	0.996	0.007	0	0	0	0.995
Road	0	0.906	0.028	0.023	0.012	0.921
Tree	0	0.045	0.922	0	0	0.938
Pole	0	0.012	0	0.964	0	0.976
Car	0	0.012	0	0	0.907	0.947
Overall segmentation accuracy: **OSACC**					0.939	
Overall classification accuracy: **OCACC**						0.955

6.3 Data Set 3

The data set consisting of $110,392$ data points was reduced to $18,541$ super-voxels keeping maximum voxel size 0.3 m and $c_D = 0.25$ m. These super-voxels are then segmented into 237 distinct objects. The classification result of these objects is shown in Figure 7 and in Table 3.

Table 3: Classification results of data set 3 in the new evaluation metrics.

	Building	Road	Tree	Pole	Car	**CACC**
Building	0.901	0.005	0.148	0	0	0.874
Road	0.003	0.887	0.011	0.016	0.026	0.916
Tree	0.042	0.005	0.780	0	0	0.867
Pole	0	0.002	0	0.966	0	0.982
Car	0	0.016	0.12	0	0.862	0.863
Overall segmentation accuracy: : **OSACC**					0.879	
Overall classification accuracy: **OCACC**						0.901

6.4 Effect of Voxel Size on Classification Accuracy

As the properties of super-voxels are constant mainly over the whole voxel length and these properties are then used for segmentation and then classification, thus their size impacts the classification process. However as the voxel size changes, the inter-distance constant c_D also needs to be adjusted accordingly.

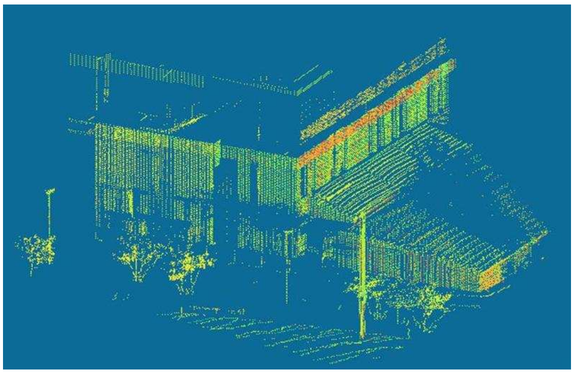

(a) 3D data points.

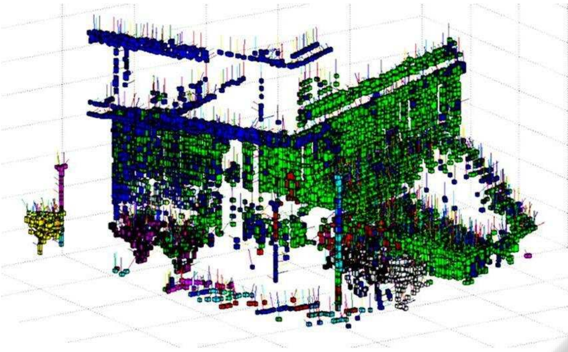

(b) Voxelisation and segmentation into objects.

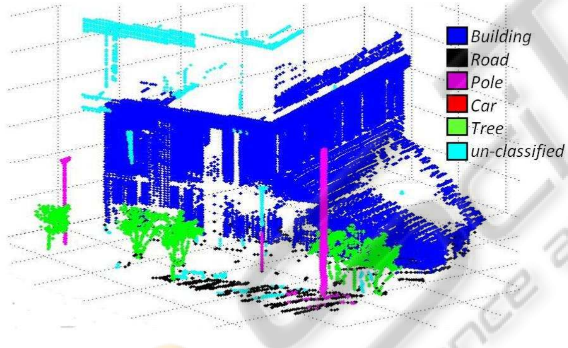

(c) Labeled points.

Figure 5: (a) Shows 3D data points of data set 1. (b) shows segmentation of 3D points. (c) shows classification results (labeled 3D points).

The effect of voxel size on the classification result was studied. The maximum voxel size and the value of c_D was varied from 0.1 m to 1.0 m on data set-1 and corresponding classification accuracy was calculated. The results are shown in Figure 8(a). Then for the same variation of maximum voxel size and c_D the variation in processing time was studied as shown in Figure 8(b).

An arbitrary value of time T_a is chosen for comparison purposes (along Z-axis time varies from 0 to $200T_a$). This makes the comparison results independent of the processor used, even though the same processor was used for all computations.

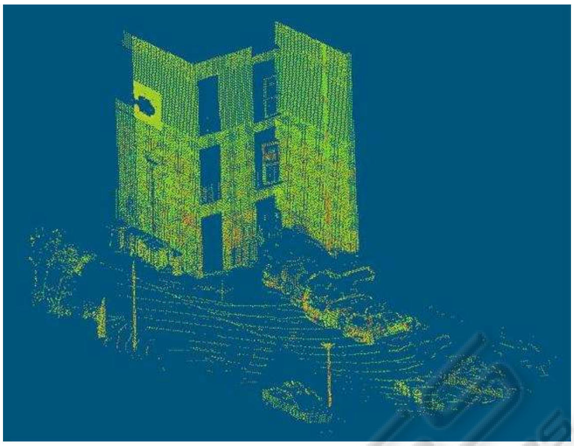

(a) 3D data points.

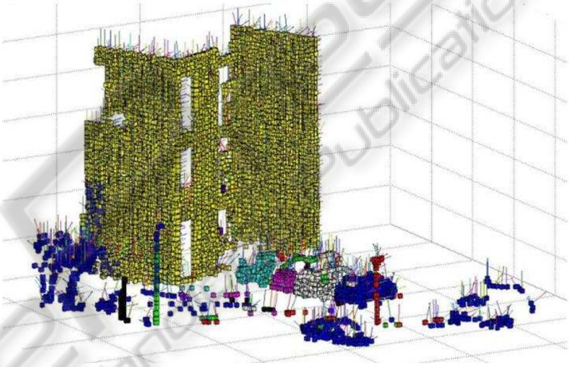

(b) Voxelisation and segmentation into objects.

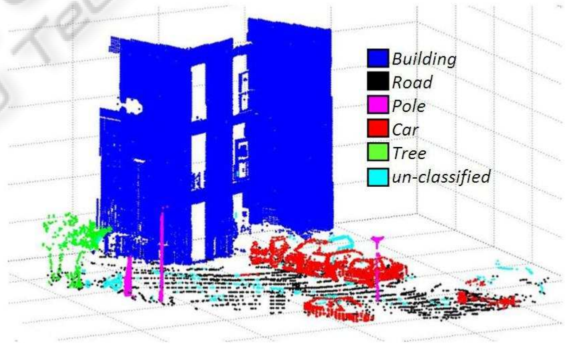

(c) Labeled points.

Figure 6: (a) Shows 3D data points of data set 2. (b) shows segmentation of 3D points. (c) shows classification results (labeled 3D points).

The results show that with smaller voxel size the segmentation and classification results improve (with a suitable value of c_D) but the computational cost increases. It is also evident that variation in value of c_D has no significant impact on time t. It is also observed that after a certain reduction in voxel size the classification result does not improve much but the computational cost continues to increase manifolds. As

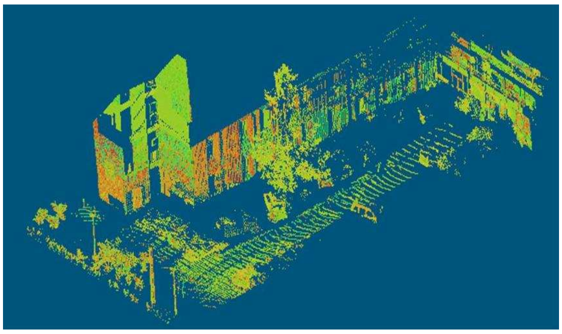

(a) 3D data points.

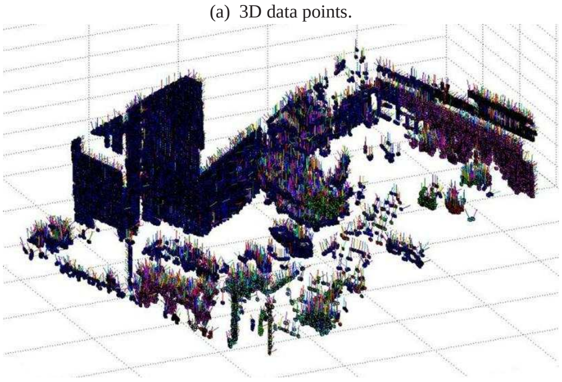

(b) Voxelisation and segmentation into objects.

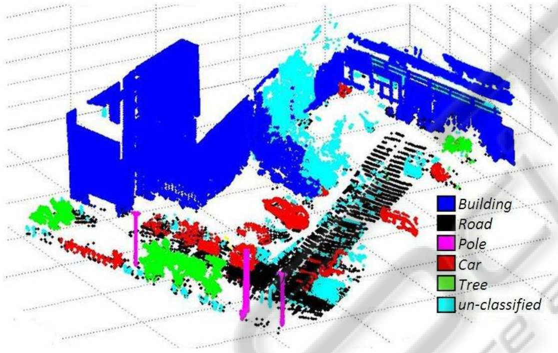

(c) Labeled points.

Figure 7: (a) Shows 3D data points of data set 3. (b) shows segmentation of 3D points. (c) shows classification results (labeled 3D points).

both **OCACC** and time (both plotted along Z-axis) are independent thus using and combining the results of the two 3D plots in Figure 8 we can find the optimal value (in terms of **OCACC** and t) of maximum voxel size and c_D depending upon the final application requirements. For our work we have chosen a maximum voxel size of 0.3 m and $c_D = 0.25\ m$.

6.5 RGB Color and Intensity

The effect of incorporating RGB Color and Intensity on the segmentation and classification results was also studied. The results are presented in Table 4.

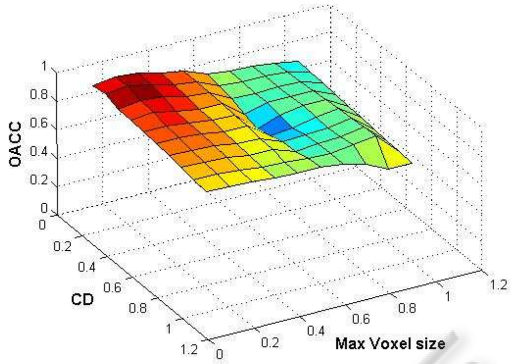

(a) Influence of voxel size on OCACC.

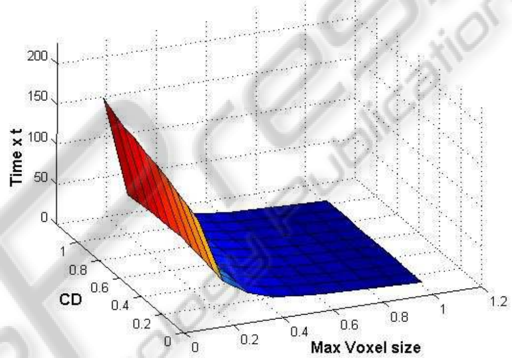

(b) Influence of voxel size on processing time.

Figure 8: (a) is a 3D plot in which the effect of maximum voxel size and variation on OCACC is shown. In (b) the effect of maximum voxel size and variation on processing time is shown. Using the two plots we can easily find the optimal value for maximum voxel size and c_D.

Table 4: Overall segmentation and classification accuracies when using RGB-Color and intensity values.

Data Set #	Only RGB-Color		Intensity with RGB-Color	
	OSACC	**OCACC**	**OSACC**	**OCACC**
#1	0.660	0.772	0.930	0.943
# 2	0.701	0.830	0.939	0.955
# 3	0.658	0.766	0.879	0.901

It is observed that incorporating RGB color alone is not sufficient in an urban environment due to the fact that it is heavily affected by illumination variation (part of an object may be under shade or reflect bright sunlight) even in the same scene. This deteriorates the segmentation process and hence the classification. This is perhaps responsible for the lower classification accuracy as seen in first part of Table 4. It is the reason why intensity values are incorporated as they are illumination invariant and found to be more consistent. The improved classification results are presented in second part of Table 4.

7 CONCLUSIONS

In this work we have presented a super-voxel based segmentation and classification method for 3D urban scenes. For segmentation a link-chain method is proposed, which is followed by a classification of objects using local descriptors and geometrical models. In order to evaluate our work we have introduced a new evaluation metric which incorporates both segmentation and classification results. The results show an overall segmentation accuracy of 87% and a classification accuracy of about 90%.

Our study shows that the classification accuracy improves by reducing voxel size (with an appropriate value of c_D) but at the cost of processing time. Thus a choice of an optimal value, as discussed, is recommended.

The study also demonstrates the importance of using intensity values along with RGB colors in the segmentation and classification of urban environment as they are illumination invariant and more consistent.

The proposed method can also be used as an add-on boost for other classification algorithms.

ACKNOWLEDGEMENTS

This work is supported by the Agence Nationale de la Recherche (ANR - the French national research agency) (ANR CONTINT iSpace&Time – ANR-10-CONT-23) and by “le Conseil Général de l’Allier”. The authors would like to thank Pierre Bonnet and all the other members of Institut Pascal who contributed to this project.

REFERENCES

Anguelov, D., Taskar, B., Chatalbashev, V., Koller, D., Gupta, D., Heitz, G., and Ng, A. (2005). Discriminative Learning of Markov Random Fields for Segmentation of 3D Scan Data. In *Computer Vision and Pattern Recognition, IEEE Computer Society Conference on*, volume 2, pages 169–176, Los Alamitos, CA, USA. IEEE Computer Society.

Douillard, B., Brooks, A., and Ramos, F. (2009). A 3D Laser and Vision Based Classifier. In *5th Int. Conf. on Intelligent Sensors, Sensor Networks and Information Processing (ISSNIP)*, page 6, Melbourne, Australia.

Douillard, B., Underwood, J., Kuntz, N., Vlaskine, V., Quadros, A., Morton, P., and Frenkel, A. (2011). On the Segmentation of 3D LIDAR Point Clouds. In *IEEE Int. Conf. on Robotics and Automation (ICRA)*, page 8, Shanghai, China.

Felzenszwalb, P. and Huttenlocher, D. (2004). Efficient Graph-Based Image Segmentation. *International Journal of Computer Vision*, 59:167–181. 10.1023/B:VISI.0000022288.19776.77.

Golovinskiy, A. and Funkhouser, T. (2009). Min-Cut Based Segmentation of Point Clouds. In *IEEE Workshop on Search in 3D and Video (S3DV) at ICCV*, pages 39 – 46.

Halma, A., ter Haar, F., Bovenkamp, E., Eendebak, P., and van Eekeren, A. (2010). Single spin image-ICP matching for efficient 3D object recognition. In *Proceedings of the ACM workshop on 3D object retrieval*, 3DOR ’10, pages 21–26, New York, NY, USA.

Johnson, A. (1997). *Spin-Images: A Representation for 3-D Surface Matching*. PhD thesis, Robotics Institute, Carnegie Mellon University, Pittsburgh, PA.

Kazhdan, M., Funkhouser, T., and Rusinkiewicz, S. (2003). Rotation Invariant Spherical Harmonic Representation of 3D Shape Descriptors. In *Proceedings of the 2003 Eurographics/ACM SIGGRAPH symposium on Geometry processing*, SGP ’03, pages 156–164, Aire-la-Ville, Switzerland, Switzerland. Eurographics Association.

Klasing, K., Althoff, D., Wollherr, D., and Buss, M. (2009). Comparison of Surface Normal Estimation Methods for Range Sensing Applications. In *IEEE Int. Conf. on Robotics and Automation*, pages 3206 – 3211, Kobe, Japan.

Knopp, J., Prasad, M., and Gool, L. V. (2010). Orientation invariant 3D object classification using hough transform based methods. In *Proceedings of the ACM workshop on 3D object retrieval*, 3DOR ’10, pages 15–20, New York, NY, USA. ACM.

Lam, J., Kusevic, K., Mrstik, P., Harrap, R., and Greenspan, M. (2010). Urban Scene Extraction from Mobile Ground Based LiDAR Data. In *International Symposium on 3D Data Processing Visualization and Transmission*, page 8, Paris, France.

Lim, E. and Suter, D. (2007). Conditional Random Field for 3D Point Clouds with Adaptive Data Reduction. In *International Conference on Cyberworlds*, pages 404–408, Hannover.

Lim, E. H. and Suter, D. (2008). Multi-scale Conditional Random Fields for Over-Segmented Irregular 3D Point Clouds Classification. In *Computer Vision and Pattern Recognition Workshop*, volume 0, pages 1–7, Anchorage, AK, USA. IEEE Computer Society.

Liu, Y., Zha, H., and Qin, H. (2006). Shape Topics-A Compact Representation and New Algorithms for 3D Partial Shape Retrieval. In *IEEE Conf. on Computer Vision and Pattern Recognition*, volume 2, pages 2025–2032, New York, NY, USA. IEEE Computer Society.

Lu, W. L., Okuma, K., and Little, J. J. (2009). A Hybrid Conditional Random Field for Estimating the Underlying Ground Surface from Airborne LiDAR Data. *IEEE Transactions on Geoscience and Remote Sensing*, 47(8):2913–2922.

Moosmann, F., Pink, O., and Stiller, C. (2009). Segmentation of 3D Lidar Data in non-flat Urban Environments using a Local Convexity Criterion. In *Proc. of the IEEE Intelligent Vehicles Symposium (IV)*, pages 215–220, Nashville, Tennessee, USA.

Munoz, D., Vandapel, N., and Hebert, M. (2009). Onboard contextual classification of 3-D point clouds with learned high-order Markov Random Fields. In *IEEE Int. Conf. on Robotics and Automation (ICRA)*, pages 2009 – 2016, Kobe, Japan.

Osada, R., Funkhouser, T., Chazelle, B., and Dobkin, D. (2002). Shape distributions. *ACM Trans. Graph.*, 21:807–832.

Pauling, F., Bosse, M., and Zlot, R. (2009). Automatic Segmentation of 3D Laser Point Clouds by Ellipsoidal Region Growing. In *Australasian Conference on Robotics & Automation*, page 10, Sydney, Australia.

Pu, S. and Vosselman, G. (2009). Building Facade Reconstruction by Fusing Terrestrial Laser Points and Images. *Sensors*, 9(6):4525–4542.

Rusu, R., Bradski, G., Thibaux, R., and Hsu, J. (2010). Fast 3D Recognition and Pose Using the Viewpoint Feature Histogram. In *IEEE/RSJ Int. Conf. on Intellig. Robots and Systems (IROS)*, pages 2155 – 2162, Taipei, Taiwan.

Schoenberg, J., Nathan, A., and Campbell, M. (2010). Segmentation of dense range information in complex urban scenes. In *IEEE/RSJ Int. Conf. on Intellig. Robots and Systems (IROS)*, pages 2033 – 2038, Taipei, Taiwan.

Sithole, G. and Vosselman, G. (2004). Experimental comparison of filter algorithms for bare-Earth extraction from airborne laser scanning point clouds. *ISPRS Journal of Photogrammetry and Remote Sensing*, 59(1-2):85 – 101. Advanced Techniques for Analysis of Geo-spatial Data.

Strom, J., Richardson, A., and Olson, E. (2010). Graph-based Segmentation for Colored 3D Laser Point Clouds. In *Proceedings of the IEEE/RSJ Int. Conf. on Intellig. Robots and Systems (IROS)*, pages 2131 – 2136.

Sun, J., Ovsjanikov, M., and Guibas, L. (2009). A Concise and Provably Informative Multi-Scale Signature Based on Heat Diffusion. In *Proceedings of the Symposium on Geometry Processing*, pages 1383–1392, Aire-la-Ville, Switzerland. Eurographics Association.

Triebel, R., Shin, J., and Siegwart, R. (2010). Segmentation and Unsupervised Part-based Discovery of Repetitive Objects. In *Proceedings of Robotics: Science and Systems*, page 8, Zaragoza, Spain.

Verma, V., Kumar, R., and Hsu, S. (2006). 3D building detection and modeling from aerial lidar data. In *Computer Vision and Pattern Recognition, IEEE Computer Society Conference on*, volume 2, pages 2213–2220, New York, USA. IEEE Computer Society.

Vieira, M. and Shimada, K. (2005). Surface mesh segmentation and smooth surface extraction through region growing. *Computer Aided Geometric Design*, 22(8):771 – 792.

Vosselman, G., Kessels, P., and Gorte, B. (2005). The utilisation of airborne laser scanning for mapping. *International Journal of Applied Earth Observation and Geoinformation*, 6(3-4):177 – 186. Data Quality in Earth Observation Techniques.

Zhu, X., Zhao, H., Liu, Y., Zhao, Y., and Zha, H. (2010). Segmentation and classification of range image from an intelligent vehicle in urban environment. In *IEEE/RSJ Int. Conf. on Intellig. Robots and Systems (IROS)*, pages 1457 – 1462, Taipei, Taiwan.